Materials Science & Engineering C 119 (2021) 111585

Contents lists available at ScienceDirect

Materials Science & Engineering C

journal homepage: www.elsevier.com/locate/msec

Engineered silica nanoparticles are biologically safe vehicles to deliver drugs or genes to liver cells

Özge Tüncel[a], Erkan Kahraman[b,c], Gülsün Bağci[b,d], Neşe Atabey[b], Serdar Özçelik[a,*]

[a] Department of Chemistry, İzmir Institute of Technology, Izmir, 35430 Urla, Turkey
[b] Izmir Biomedicine & Genome Center(IBG), Izmir, 35340, Balcova, Turkey
[c] Atatürk Sağlık Hizmetleri Meslek Yüksekokulu, Ege University, Izmir, 35040, Bornova, Turkey
[d] Dokuz Eylül University, Izmir International Biomedicine and Genome Institute, Izmir, 35340, Balcova, Turkey

ARTICLE INFO

Keywords:
Liver
Liver cancer
Silica nanoparticles
Cytotoxicity
Genotoxicity
Hemolysis
Colony formation
Cell-cycle
Mitochondrial membrane potentials

ABSTRACT

Engineered silica nanoparticles (SiNP) are emerging materials for medical applications. Evaluating biological responses of specific cells treated with engineered silica nanoparticles is however essential. We synthesized and characterized the physicochemical properties of silica nanoparticles with two different sizes of 10 and 100 nm (10SiNP and 100SiNP) dispersed in cell culture medium. HuH-7, an epithelial-like human hepatoblastoma cell line and SK-HEP-1, a liver sinusoidal endothelial cell line (LSEC) are employed to evaluate their biological responses for the SiNP treatment. Primary human lymphocytes are used to assess genotoxicity recommended by OECD guidelines while erythrocytes are used to assess hemolytic activity. The engineered silica nanoparticles are not able to produce radical species, to alter the mitochondrial membrane potential, and induce any adverse effects on cell proliferation. The colony formation ability of HuH-7 hepatoblastoma cells was not affected following the SiNP treatment. Furthermore, SiNPs do not induce hemolysis of red blood cells and are not genotoxic. These findings suggest that SiNPs regardless of the size, amount, and incubation time are biologically safe vehicles to deliver drugs or genes to the liver.

1. Introduction

Silica nanoparticles (SiNP) are promising materials for medical and biological applications such as a non-viral vehicle for gene and drug delivery [1–3]. A phase-I study was performed using luminescent colloidal silica nanoparticles named as “Cornell dots”. Dose responses of the Cornell dots coated PEG (polyethylene glycol) and RGD peptides were evaluated for five melanoma patients [1]. PEG-coated silica core-gold shell nanoparticle, called AuroLase, are in phase trials for the laser ablation treatment of solid tumors [2].

The synthetic chemistry of silica nanoparticles is very mature but their preparation methods for in-vitro studies vary substantially. A recent study conducted in several laboratories in-parallel [4] discussed how to prepare nanoparticles for in-vitro toxicity testing. It was demonstrated that silica nanoparticles re-dispersed in media such as DMEM or RPMI affect cell viability and induce toxicity for HeLa and U937 cells [5]. Furthermore, assay conditions and controls are shown to be equally important along with physicochemical characterizations [6]. It was highlighted that the nanoparticles were aggregated or agglomerated in the cell culture medium. When the size of amorphous silica nanoparticles is large it reduces cell viability [7]. When nanoparticles are injected into an animal intravenously their surface is rapidly covered with a layer of blood proteins called protein corona [8] if they are not capped with PEG. Undesirable protein adsorption on nanoparticle surfaces makes particles larger and reduces circulation times in blood [9]. Lack of standardized preparation procedures of nanoparticles as well as insufficient characterization of nanomaterials in biological media may lead to incompatible results.

Hepatocytes are specialized cells to eliminate foreign materials from the human body by enzymatic breakdown or excretion into the bile [3]. SiNPs larger than 7 nm were mostly accumulated in kidneys, liver, and spleen both in mouse and human [10]. For safe clinical applications, nanoparticles must be non-toxic, effectively targeting diseased cells and should have a good clearance profile. Since nanoparticles are accumulated in liver tissue, as a result, they will actively interact with liver cells. However, a few studies collectively discuss the impact of physicochemical parameters of SiNPs on cytotoxic and genotoxic patterns of cell lines [11]. HuH-7, an epithelial-like human hepatoblastoma cell line, and SK-HEP-1, a liver sinusoidal endothelial cell line may provide a better model system because of a combination of epithelial cancer and

* Corresponding author.
E-mail address: serdarozcelik@iyte.edu.tr (S. Özçelik).

https://doi.org/10.1016/j.msec.2020.111585
Received 1 May 2020; Received in revised form 4 September 2020; Accepted 24 September 2020
Available online 30 September 2020

endothelial cells together. A liver model combining HuH-7 and SK-HEP-1 cells was explored to evaluate biological effects induced by engineered SiNPs. Furthermore, blood cells lymphocytes and erythrocytes are used to assess genotoxicity and hemolytic responses, respectively.

A literature survey provided in the supplementary information-1 (Fig. S1 and Table S1) summarizes that biological responses of a variety of cells vary greatly with respect to size and amount of nanoparticles, but no trend can be concluded. This survey recommends that the assessment of biological responses for each cell type must be completed. In addition, nanoparticles smaller than 10 nm are cleared by the kidney and larger particles are cleared by the hepatobiliary system. Therefore, to stimulate the clearance of nanoparticles by the hepatobiliary system we used 10SiNP and 100SiNP to evaluate biological responses of liver cancer cells. Human blood cells are also used to assess hemolytic responses and genotoxicity. The overall evaluations suggest that SiNPs are promising as non-viral vehicles to deliver drugs or genes to liver.

2. Methods

2.1. SiNP (silica nanoparticle) synthesis

10SiNP and 100SiNP were synthesized based on a modified Stöber method [12]. Tetraethylorthosilicate (TEOS) (99.999% trace metals basis), ethanol (EtOH-ACS Grade) and ammonia solution (98%-ACS, Reag. Ph Eur) were purchased from Sigma-Aldrich Co. and used without purification. Briefly, to prepare 100 nm size particles 30 ml of absolute ethanol was mixed with 1.85 ml of 0.443 M NH_4OH and stirred for 5 min. 1.2 ml of 0.175 M TEOS was added to the solution under N_2 (g). The solution was stirred for 20 h at room temperature. Followingly, 0.245 ml of 1.1 mM TEOS was added into the dispersion to improve the colloidal stability of SiNPs. FITC (fluorescein isothiocyanate ($\geq$90%, HPLC)) doped silica nanoparticles were synthesized by the same method. FITC conjugated APTES (99%) as a precursor used along with TEOS at the beginning. The 10SiNP nanoparticles were synthesized and precipitated by ultracentrifugation at 50.000 RPM for 18 h using Optima Max XP ultracentrifugation (Beckman Coulter) with MLA-55 rotor and quick-seal polyallomer tubes. 100SiNPs were precipitated and collected by centrifugation at 6000 RPM for 15 min. Supernatants were removed and precipitates were washed with ethanol in order to remove unreacted reagents from the synthesis media.

The 10SiNPs are colloidally stable for several months and several weeks for 100SiNPs (physical observation). When the powdery silica nanoparticles were re-dispersed in the cell culture medium, we observed that the resulting SiNP dispersions are not agglomerated nor precipitated for several weeks.

2.2. Physicochemical characterization

Hydrodynamic size and zeta potential of SiNPs dispersed in Dulbecco's Modified Eagle Medium (DMEM) with Fetal Bovine Serum (FBS) were measured by using Zetasizer NanoZS (Malvern Instruments Ltd.). Drop-cast films of 10SiNPs and 100SiNPs were analyzed by Transmission Electron Microscopy (JEOL JEM-ARM200F UHR and Zeiss Sigma 500) to examine size, shape and uniformity of the particles. Elemental analysis of SiNP was performed by Energy Dispersive X-Ray Spectroscopy (Philips XL-30S FEG Scanning Electron Microscopy) at 5.0 kV. Fourier Transformed Infrared Spectroscopy (Perkin Elmer Spectrum 100) was used to confirm nanoparticle formation. X-Ray diffraction measurements (Philips X'Pert Pro) were performed to calculate the number of particles per milligram. Peak-search and search-match analysis by X'Pert software (Philips Analytical) was used to determine the crystalline form of SiNP. NMR experiments were performed with a Bruker 400 MHz spectrometer and a Bruker Avance 500WB spectrometer.

2.3. Cell culture

HuH-7 and SK-HEP-1 cell lines were kindly provided by Prof. Mehmet Öztürk (IBG, Izmir, Turkey). Cells were maintained in DMEM containing 10% FBS, 2 mM L-Glutamine, 100 U/ml penicillin, 0.1 mg/ml streptomycin and 1% (*v*/v) non-essential amino acids solution in a humidified 5% CO_2 incubator at 37 °C [13]. Primary human lymphocytes obtained from a healthy male donor were used to assess genotoxicity according to OECD guidelines.

2.4. Viability tests

MTT (3-(4,5-Dimethylthiazol-2-yl)-2,5-diphenyltetrazolium bromide) and Sulforhodamine B tests were performed to evaluate the cell viability upon the nanoparticle treatments of the cells [14]. HuH-7 and SK-HEP-1 cells were plated at a density of 1000 cells per well in flat-bottom 96-well plates allowed to grow overnight prior to the exposure to SiNPs at different concentrations. After 24 h, the cells were treated with 0.2, 2.0, 20.0, 200.0 μg/ml nanoparticles (1.4×10^{15} and 1.4×10^{12} particles/ml equivalent to 1.0 mg/ml of 10SiNP and 100SiNPs, respectively) suspended in 100 μl DMEM. 1.0 mM hydrogen peroxide solution was used as a positive control. 15.0 μl of MTT was added (5 mg/ml) into the wells and the plates were incubated at 37 °C for 4 h. The medium containing MTT solution was replaced with DMSO and incubated for 30 min at room temperature. The plates were shaken for 10 min to solubilize formazan crystals. The absorbance was measured by a Varioskan spectrophotometer at both 570 nm and 720 nm. The SRB assay was performed according to instructions of the TOX6 kit (Sigma-Aldrich). At the end of the incubation period, the cells were fixed with 25 μL 50% ice-cold trichloroacetic acid (TCA) and incubated in the dark at 4 °C for 1 h. TCA was washed with dH_2O and cells were stained with 50 μl of 0.4% Sulforhodamine B (SRB) solution in 1% acetic acid solution after drying period. The plates were incubated in the dark for 20 min at room temperature. The unbound dyes were washed away using 1% acetic acid and the plates were left to air dry. The SRB was then solubilized using 100 μl of 10 mM Tris- base and OD values were measured at 510 and 565 nm. Background was measured at 690 nm.

2.5. Confocal imaging

HuH-7 and SK-HEP-1 cells were plated on glass bottom Petri dishes (Ibidi plates) for live cell imaging of mitochondria by a spinning disc confocal microscope, Andor Revolution system equipped with Olympus IX71 and Okolab stage incubator system. Cells were treated with FITC-doped 100SiNP nanoparticles (20 and 200 μg/ml) to determine locations of nanoparticles in the cytoplasm. Mitochondria were stained by 200 nM Mitored (Sigma Aldrich) in the presence and absence of SiNPs. Lysosomes were stained by 75 nM Lysotracker DND-99 (Thermo Fisher Scientific) to determine colocalization of SiNPs with lysosomes. Coherent Innova diode lasers operating at 488 nm and 532 nm were used to excite FITC-doped SiNPs, for lysosomal and mitochondrial imaging, respectively. Emission filters of 530/50 nm and 560/30 nm were used to collect images.

2.6. Image analysis

2.6.1. Mitochondrial intensity analysis

The images were analyzed by using Image J platform. The area of the cells was determined by DIC contrast images. Fluorescence counts were measured to assess change in the mitochondrial membrane potential (MMP). The cell membrane boundary as a region of interest (ROI), was sketched by hand using the polygon tool. ROI Manager was used to calculate cell area. The histograms of all ROIs were transferred into Microsoft Excel. The counts were calculated by multiplying the bins times bin values of each ROI saved. Grand total count for the MMP

of one cell was determined by summing all counts. Several mitochondria in one image were assessed. The total count of MMP in a single cell was divided by cell area to eliminate variability of cell size.

2.6.2. Imaging of reactive oxygen species

The reagent 2′,7′-dichlorofluorescin diacetate (DCFDA) (Sigma Aldrich-97%) was used to determine hydroxyl, peroxyl and other reactive species within the cell [15]. The cells were cultured in 8-well ibidi chambers before silica nanoparticle treatment. Non-fluorescent 10SiNP and 100SiNP were used instead of FITC-doped SiNPs to prevent spectral overlap with DCFDA. The cells were incubated with 200 μg/ml of SiNPs up to 24 h and stained with 1.0 μg/ml DCFDA for 30 min. The cells were imaged immediately following the staining to determine the presence of ROS in the cells. Hydrogen peroxide treated cells were used as a positive control group. The ROIs were sketched for individual cells and their intensity histograms were collected. Total counts were measured to determine the presence of ROS.

2.6.3. Colocalization analysis

Colocalization of SiNPs with lysosomes and mitochondria were determined using Pearson correlation coefficients analysis was performed using coloc plug-in in a Fiji platform (Image J) [16]. The pixel-shift correction and calibration were made using calibrated, commercially available fluorescent polystyrene spheres (green/yellow emitting 100 nm sized particles). The individual cellular areas were established as described in the mitochondrial intensity analysis part.

2.7. Flow cytometry

The cells incubated with SiNPs were collected by trypsinization and washed twice with ice-cold PBS. The ethanol-suspended cells were centrifuged for 5 min at 300 *g*. The cells were permeabilized in 0.1% Triton X-PBS solution after fixation in ice-cold 75% ethanol. DNA was stained with 0.1 mg/ml propidium iodide (PI) for 15 min. The cells were transferred into flow cytometer tubes and assayed with FACSCanto Flow cytometer (Becton Dickinson) [17]. To detect PI emission, a solid-state laser at 488 nm was used for excitation. A combination of 556/LP and 585/40 BP emission filters was used for detection. Results were analyzed with FACS Diva Software v5.0.3 (Becton Dickinson) and ModFit LT 3.0 programs.

2.8. Genotoxicity test

Cytokinesis-blocked micronucleus assays were performed for assessment of genotoxicity [18]. Briefly, peripheral blood sample (~8 mL) was obtained by venipuncture from a healthy male volunteer (29 age, non-smoker, not affected by radiation, and not under any medication) into Vacutainer CPTTM tubes (BD Cat: 362761). The leukocyte suspension was processed according to the manufacturer's instructions. After resuspension, centrifugation and washing steps, lymphocyte pellet was suspended at a concentration of 10^6cell/750 μl in RPMI-1640 medium supplemented with 20% FBS, 2 mM L-Glutamine, 2.4 μg/ml phytohemagglutinin L, 100 units/ml penicillin and 100 μg/ml streptomycin, and incubated at 37 °C in a humidified atmosphere of 5% CO_2 [19]. 24 h later various concentrations of the SiNPs (0, 0.2, 2, 20 μg/ml) were added. Cytochalasin-B (Cyt−B) was added to obtain a final 4.5 μg/ml concentration into culture suspension at the 44th hour of incubation and incubated for a further 28 h. At the end of the incubation, Cyt-B solution was discarded, the cells were harvested for slide preparation and stained with Giemsa. The cells were imaged with 1000× magnification to determine micronucleus number in each of the duplicate cultures (total 2000 BN cells/conditions). To determine DNA damage and/or chromosomal instability, micronuclei (MNi), nucleoplasmic bridge (NPB) and nuclear bud (NBUD) numbers were scored in binucleated cells that have equal size, similar staining pattern, and intensity [18]. Mitomycin C (MMC), 0.1 μg/ml, was used as a positive control. Nuclear division index (NDI) was calculated according to the method of Eastmond and Tucker [20]. Results were statistically analyzed by using One Way ANOVA and post hoc Tukey.

2.9. Hemolysis assay

Blood obtained from young healthy males who gave consent to participate in this study at the Dokuz Eylül University Blood Bank, Izmir, Turkey and they were stored at +4 °C for 24 h. Blood samples were collected into BD Vacutainer 10 mL Heparin tubes. Blood samples were pooled and three replicas of each condition were prepared. SiNPs were gently vortexed before experiment then 0.2 μg/ml, 2 μg/ml, 20 μg/ml and 200 μg/ml serial dilutions of 10SiNP and 100SiNP were prepared firstly. 700 μl SEROX DPBS Ca^{2+} w/o, Mg^{2+} w/o, 100 μl serial diluted 10SiNP and 100SiNP of each concentration, 100 μl blood or positive/negative controls were added into labeled corresponding eppendorfs. For negative controls only DPBS and complete DMEM, for positive control 100 μl of 10% Triton-X-100 (v/v) diluted with water were used. Eppendorfs were mixed gently and they were placed into a 37 °C water bath for 3 h. Tubes were mixed gently every 30 min during incubation. Tubes were evaluated before centrifugation and after centrifugation for 15 min at 800 *g*. Supernatants obtained were added into 96-well plates as duplicates for each replicate. OD were measured at 540 nm spectrophotometrically. Results were calculated by Microsoft Excel and their statistical analysis was performed via Graphpad Prism8. Hemolysis assay was performed according to protocols of Dobrovolskaia et al. 2008 after some modifications [21].

2.10. Clonogenic assay

12-well plates were coated with 0.01 mg/ml poly-D-Lysine (Sigma Aldrich) and they were incubated at RT for 30 min in the Class II cabinet. Then plates were washed with sterile ultrapure water and were dried O/N at RT. 100 cells per well SK-HEP-1 cells were seeded on the poly-D-Lysine coated plates at least triplicate and incubated at 37 °C in 5%CO_2 conditions for 24 h. Then cells were treated with 0 μg/ml, 2 μg/ml, 20 μg/ml and 200 μg/ml concentration of both 10SiNP and 100SiNP for 24 h. Cells were washed with 1× PBS twice and they were cultured 14 days after SiNP treatment. Then cells were washed with 1× PBS and they were fixed with 75% methanol and 25% glacial acetic acid mix for 5 min at RT. They were stained with 0.5% Crystal violet solution prepared with distilled water (Sigma Aldrich) for 2 h at RT. Plates were washed with distilled water and they were air dried at RT. Plates were imaged under Molecular Imager® Gel Doc™ XR+ System with Image Lab™ Software (BIO-RAD) by using white Light Conversion Screen. Colony numbers were counted under microscopy and cell numbers were higher than 100 cells considered as colonies. Experiments were repeated at least two times. Clonogenic assay was performed based on protocol published by Yang et al. [22].

3. Results

3.1. The physicochemical parameters of SiNPs

The size distributions were provided in Fig. 1(A and B). The size distributions of 10SiNPs and 100SiNPs in EtOH are narrow: the particle sizes are respectively 11 ± 2 nm and 92 ± 19 nm for 10SiNPs and 100SiNPs. Purified SiNPs while wet were redispersed in DMEM + FBS and DLS measurements were repeated. The size of nanoparticles was subtly larger due to the biological contents of the culture media as expected. The sizes of 10SiNPs and 100SiNPs are respectively 29 ± 6 nm and 107 ± 28 nm in DMEM + FBS media. The zeta potential distributions were displayed in Fig. 1C and D. The average zeta potentials of 10SiNPs and 100SiNPs were −14 ± 41 and −35 ± 36 mV in EtOH respectively. Despite the SiNPs having different zeta potential in EtOH, the zeta potentials of the two particles in the

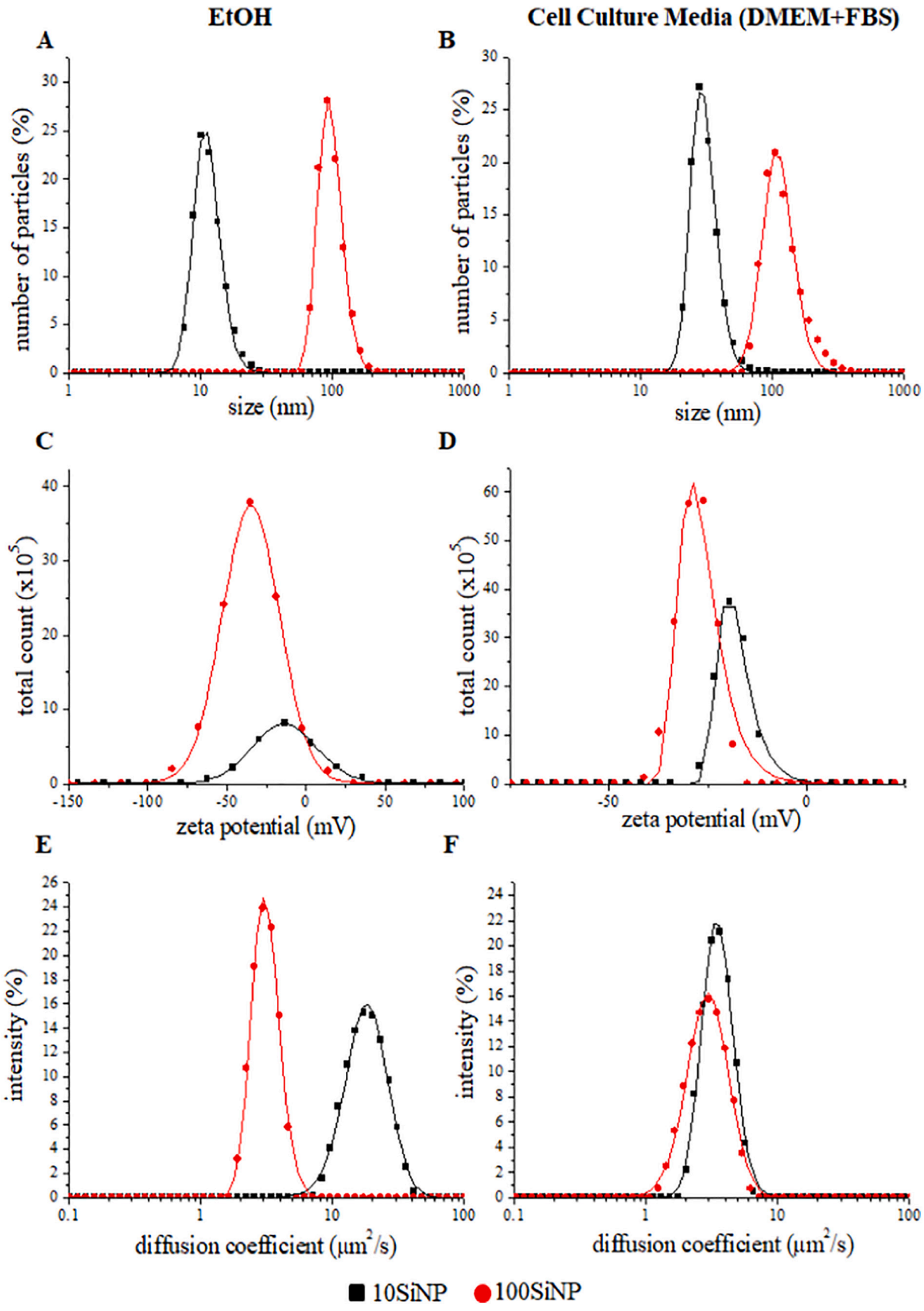

Fig. 1. Particle size distributions of 10SiNP (black) and 100SiNP (red) were shown as number distributions in EtOH (left panel) and cell culture media (right panel). Zeta potentials (C and D) and diffusion coefficients (F and G) of the silica nanoparticles were provided. Curve fittings (using extreme fit) by using Origin were applied to the data given here. (For interpretation of the references to color in this figure legend, the reader is referred to the web version of this article.)

culture medium were similar; −20 ± 4 and −29 ± 5 mV. The size of particles was inversely proportional to diffusion coefficients based on the Stokes-Einstein equation. The diffusion coefficients of 10SiNPs and 100SiNPs dispersed in EtOH and DMEM were measured 18 ± 7 and 3 ± 1 $\mu m^2/s$ respectively, as shown in Fig. 1E and F. The diffusion coefficients of 100SiNPs in EtOH and DMEM were identical, 3 ± 1 $\mu m^2/s$, indicating that the effect of protein adsorption on 100SiNP is limited.

TEM images of SiNPs showed uniformed and spherical shaped nanoparticles (given in Supplementary Information 2-Fig. S2). The structural composition of the powdery samples of 10SiNP and 100SiNPs were analyzed. SiNP powders were composed of silicon (47%) and oxygen atoms (53%) (Supplementary Information 2-Table S2 and Fig. S3).

FTIR spectra showed asymmetric vibration of Si-O-Si (1090 cm^{-1}) and asymmetric vibration of Si-OH (950 cm^{-1}) bands validating the formation of silica nanoparticles. The vibration frequencies of Si-O-Si and Si-OH for both particles were similar, but intensities were varied. The absorption bands at 2980 cm^{-1} (CH_3) and 2930 cm^{-1} (CH_2) in the TEOS spectrum disappeared in the FTIR spectra of silica nanoparticles verifying that TEOS molecules converted to the silica nanoparticles (polymerization of Si-O-Si bonds). Absorption bands of molecular water between 3300 cm^{-1} and 3500 cm^{-1} and the band at 1635 cm^{-1} assigned to O—H stretching were observed.

^{13}C CP-MAS NMR measurements were performed to show the presence of ethoxy and aminopropyl groups of the (organo)-alkoxysilanes. NMR measurements along with microscopic and spectroscopic measurements identified the formation of siloxane bonds and silica particle formation (Fig. S3—C and D).

The XRD pattern of SiNPs was compatible with tetrahedral α-cristobalite structure. We estimated the volume, mass, and number of 10SiNP and 100SiNP nanoparticles in 1.0 mg of powder by using numerical data of the α-cristobalite lattice structure and dimensions. The number of nanoparticles for 10SiNP and 100SiNP were determined to be 1.4×10^{15} and 1.4×10^{12} particles per milligram, respectively. EDS analysis confirmed that samples contained 47% of Si atoms. The XRD pattern and calculations were provided in the Supplementary Information Fig. S4.

3.2. MTT and SRB tests

The cells were incubated with up to 200 μg/ml; 2.8×10^{14}/ml particles for 10SiNPs and 2.8×10^{11} of particles/ml for 100SiNPs, respectively. Mitochondrial activity of HuH-7 cells was not affected by either 10SiNPs or 100SiNPs up to 120 h (Fig. 2). Viability of SK-HEP-1 cells was similar to the controls at 120 h for 10SiNPs. SK-HEP-1 cells seemed to be affected in the presence of 100SiNPs with 2, 20 and 200 μg/ml at 72 h however the 100SiNPs did not exhibit long-term effects on SK-HEP-1 cells. As a positive control, hydrogen peroxide induce cytotoxicity and decreased the mitochondrial activity at 1.0 mM concentration for 120 h of incubation time and independent of the cell line, validating the assessment method of the cell viability. Differences in cell proliferation between cells were analyzed by ANOVA for repeated measurements within GraphPad Prism and no significant differences were determined between SiNPs treated and untreated cells in any conditions used ($p < 0.05$). SRB data confirmed the results obtained by MTT test (data available upon request).

3.3. Confocal imaging of organelles

Figs. 3 shows locations of FITC-conjugated SiNPs in the cytoplasms. FITC-conjugated SiNPs were mostly colocalized with lysosomes compared to mitochondria for 10SiNPs and 100SiNPs in HuH-7 cells (Fig. 3A–D). The colocalization scores were varied between 0.4 and 0.9 for lysosomes and 0.2–0.6 for mitochondria (Fig. 3C). Lysosomal distributions were nearly the same for both SiNPs in HuH-7 cells, On the other hand, the mitochondrial colocalization degree for the 100SiNP (Fig. 3D) was lower than the 10SiNPs. Lysosomal colocalization values were similar for 10SiNPs and 100SiNPs in SK-HEP-1 cells (Fig. 3E–H). Mitochondrial colocalization for the 10SiNPs and 100SiNPs were varied in 0.2–0.5 and 0.0–0.3, respectively. The colocalization values of the 10SiNPs and 100SiNPs were statistically significant for both cell lines ($p < 0.0001$).

Mitochondrial membrane potentials (MMP) at single cell level were evaluated. The total intensity representing all mitochondria in one single cell were measured. Green and blue colored circles indicate the MMP intensities of control and SiNP treated single cells, respectively and red colored circles are for hydrogen peroxide treated cells (Fig. 4A–F). The cell areas and the intensities corresponding MMP were decreased for both cell lines treated with hydrogen peroxide. The MMPs of the HuH-7 cells treated with 10SiNPs are higher than the cells treated with 100SiNPs. However, the MMPs and the cell areas were not significantly altered after SiNP treatment compared to the control group. But significant heterogeneous responses of the depending of the size were observed. We noticed a sub-group (higher intensity with lower cell area) representing the cells in a phase of division appeared. The scatter graph showed that the area of the SK-HEP-1 cells slightly reduced compared to HuH-7 cells after hydrogen peroxide treatment. These findings validate that SiNP does not induce any change on the mitochondria, confirming the MTT assays.

3.4. ROS imaging

Increased oxidative stress due to treatments leads to permanent cell damage and may be observed by measuring the ROS activity. Mitochondrial activity and nanoparticle toxicity can be evaluated by measuring the level of ROS if the internalized nanoparticles induce the oxidative stress. The DCF intensity was very low in non-treated cells (negative control) but clearly detectable for both cell types treated with the peroxide (Fig. 5A and B). SiNPs treated cells showed similar physiological responses for the non-treated HuH-7 cells. The DCF fluorescence for non-treated SK-HEP-1 cells was higher than non-treated HuH-7 cells. The basal ROS activity level was a little higher for SK-HEP-1 cells compared to HuH-7 cells. The ROS level as DCF intensity for control and treated cells were illustrated in Fig. 5C and D. The DCF intensity was increased in the peroxide treated cells but not changed for the SiNP treated and control cells. In conclusion, ROS was not elevated by the SiNP treatment.

3.5. Flow cytometry

To investigate the effects of SiNPs on cell cycle progression, the cell-cycle analysis was performed by flow cytometer. 10SiNPs and 100SiNPs did not change the percentage of G1 and G2 phases cells, in comparison to the untreated cells up to 200 μg/ml for both HuH7 and SK-HEP-1 cells ($p < 0.05$) (Fig. 6A–D).

3.6. Genotoxicity test

Representative images for the formation of mononucleated, binucleated, trinucleated, multinucleated cells, MNi in the binucleated cell, NPB and NBUD were shown in Fig. 7(A–H). No significant differences in the number of MNi, NPI and NBUD formations in peripheral lymphocytes was observed in SiNP treated conditions compared to untreated ones ($p > 0.05$) suggesting that neither the size nor the amount of SiNPs induced genotoxicity (Fig. 7 and Table S3). NDI frequency was calculated approximately 2 and nearly constant after SiNP treatment of lymphocytes. The results demonstrated that the cells were divided at least once and no abnormalities after cytokinesis-block. Micronucleus number per 1000 binucleated cells was not statistically changed. MMC treatment significantly ($p > 0.001$) increased MNi, NBUD and NPB numbers shown in Fig. 7A–F. Micronucleus frequency and statistical

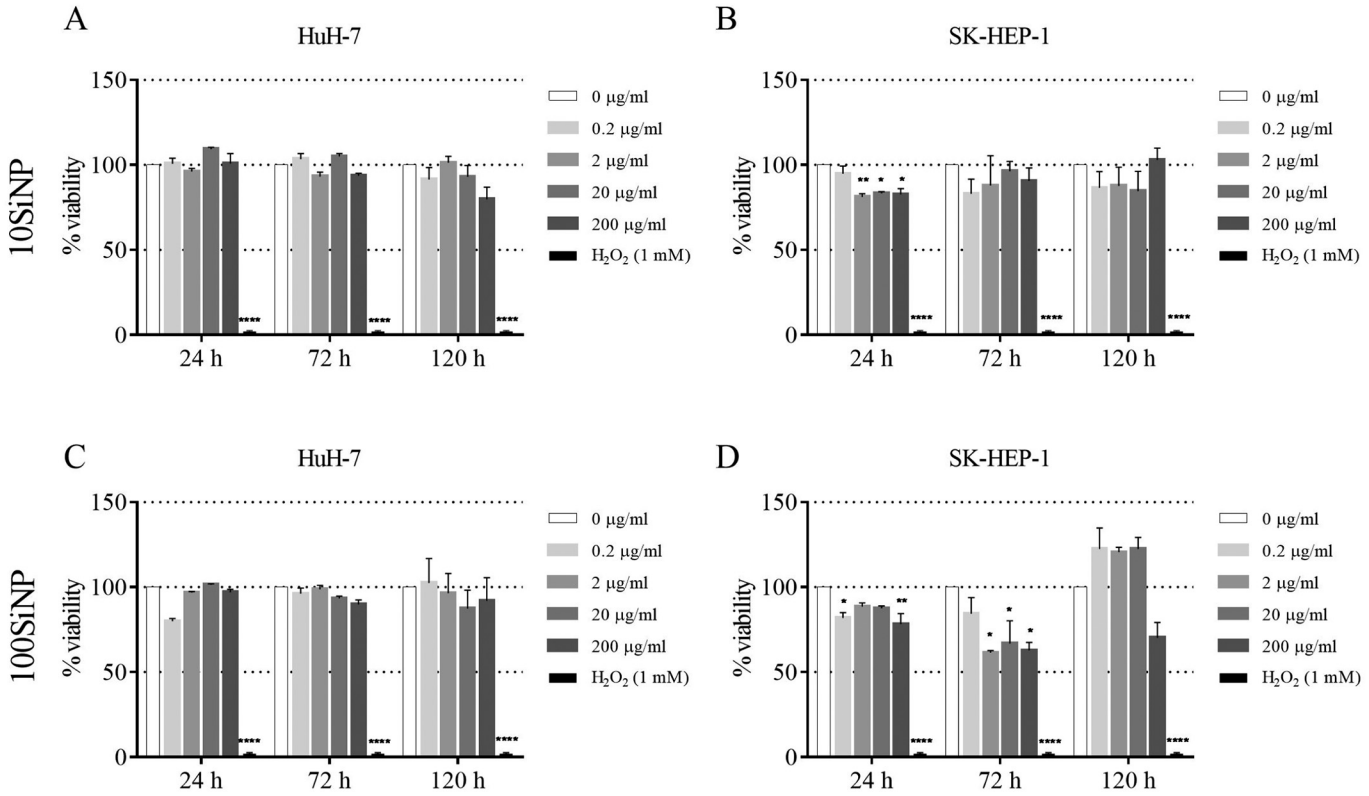

Fig. 2. The cytotoxicity of 10SiNPs and 100SiNPs were analyzed by using MTT assay. The HuH-7 (A and C) and SK- HEP-1 (B and D) cell lines were exposed with 0.2–200 μg/ml of SiNPs up to 120 h. 1 mM of hydrogen peroxide (H_2O_2) was used as a positive control. The viability was expressed by percent as comparing the control. Error bars represented the standard deviations for $n = 4$. Statistical significance indicated by the p value (**** = $p < 0.0001$).

data were summarized in Supplementary Information-2, Table S3—I and S3-II.

3.7. Hemolysis assay

Both 10 nm and 100 nm SiNPs enter the blood and get in contact with red blood cells. To assess the impact of SiNPs on erythrocyte, hemolysis test was performed by spectrophotometric measurement of hemoglobin release after exposure to various concentrations (0.2–200 μg/ml) of 10SiNPs and 100SiNPs (Fig. 8A and B top panel). The performance of hemolysis assay was tested by the negative controls (DMEM and DPBS) and positive control Triton-X-100. The hemolytic activity of 10SiNPs and 100SiNPs did not cause any hemolysis in any concentration tested (Fig. 8A and B bottom panel). Whereas Triton X-100 caused hemolysis after 3 h incubation both before and after centrifugation steps (Supplementary Fig. S5).

3.8. Clonogenic assay for SK-HEP-1 cells

SK-HEP-1 cells treated with 2 μg/ml, 20 μg/ml, 200 μg/ml SiNPs and untreated controls were grown in fresh culture medium for 14 days and their colony formation capacities were examined after they were stained with 0.5% crystal violet solution. Colony numbers which had equal or more than 100 cells were counted under a microscope (Fig. 8C and D). As shown in Fig. 8C and D, there were no statistically significant differences between colony numbers of 0 μg/ml, 2 μg/ml, 20 μg/ml, 200 μg/ml both for 10SiNP and 100SiNP ($p < 0.05$) suggesting that both 10 nm and 100 nm SiNPs that we produced do not affect colony formation of SK-HEP-1 cells.

4. Discussion

4.1. Physicochemical parameters of SiNPs

Controversial reports dominate the literature as discussed in the introduction and demonstrated in the supporting section, therefore, it is necessary to evaluate the biological responses of each cell type treated with silica nanoparticles. We combined HuH-7 hepatoblastoma and SK-HEP-1 LSEC cells together as a liver model to assess effects of SiNPs.

We chose two specific nanoparticles: 10SiNP and 100SiNP because both of them can be eliminated by the hepatobiliary system. The 10SiNPs and 100SiNPs are enlarged to 29 and 107 nm respectively because of a corona layer formation in the cell culture media. The zeta potentials of 10SiNP and 100SiNP are respectively −29 and − 20 mV at the pH of 7.4. Since the surface areas of these particles are substantially different, we normalized the zeta potentials to their surface areas and obtained $-2.72\ \mu V/nm^2$ and $-0.17\ \mu V/nm^2$ for 10SiNP and 100SiNP, respectively. Therefore, presuming the zeta potential is homogeneously distributed on the particle surface, the 10SiNPs have larger negative potential per nanometer-square. The 10SiNP has much higher zeta potential (16× larger) but has barely a higher diffusion coefficient (1.2× higher) compared to the 100SiNP. Thus, the interaction strength of 10SiNP is expected to be much stronger compared to 100SiNP. Since the cell membrane is fluidic, mobility of particles will be important for the interactions, slower the diffusion the longer the interaction time of particles with cell membranes. The diffusion coefficients of 10SiNP and 100SiNP in DMEM/FBS are similar; 3.4 and $2.9\ \mu m^2/s$, respectively. In this regard, local membrane viscosity and microenvironment play a role in particles' mobility. If the magnitude of local viscosities is not differential, the particles with different sizes but similar diffusion coefficients will be driven by the same forces. Successively, the zeta potential and the membrane potential control the interactions and will determine the fate of the particles. More 10SiNPs

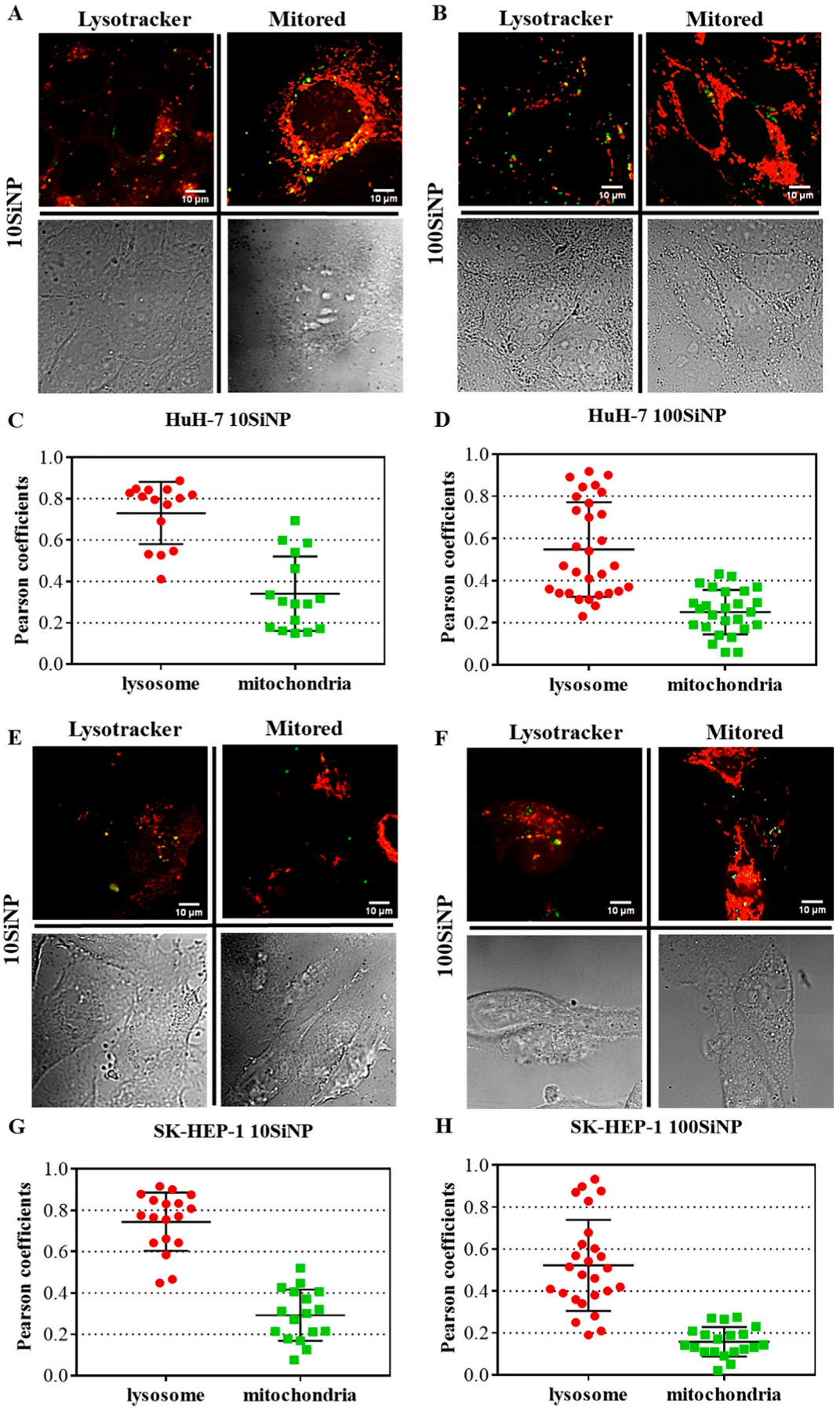

(caption on next page)

Fig. 3. The uptake of 10SiNPs and 100SiNPs was assessed by confocal imaging after 24 h incubation. The HuH-7 (panels in A and B) and SK-HEP-1 (panels in E and F) cells were stained by mitored and lysotracker dyes after SiNP treatment. Silica particles are colored green, mitored and lysotracker stained mitochondria and lysosomes are colored red. The degree of the colocalization of SiNPs with the organelles was determined by the Pearson coefficients (using ImageJ) and was graphed for HuH-7 cells and SK-HEP-1 cells (C, D and G, H). (For interpretation of the references to color in this figure legend, the reader is referred to the web version of this article.)

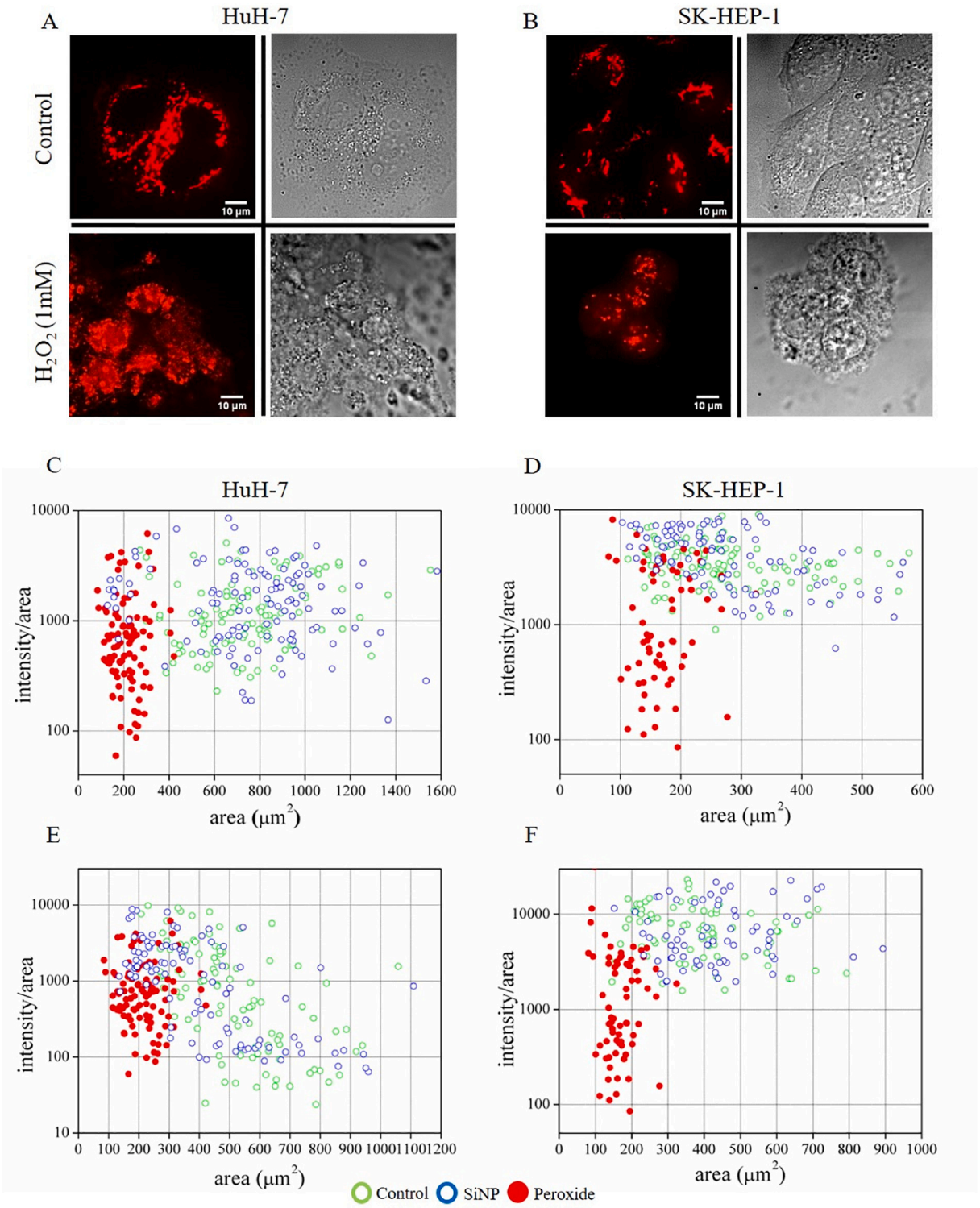

Fig. 4. Mitochondrial populations stained with mitored (red) were visualized by live cell imaging confocal microscopy. Untreated cells were used as control. Hydrogen peroxide (1.0 mM) treated HuH-7 (panels in A) and SK-HEP-1 (panels in B) cells were represented as positive control. The graphs indicated the intensity distribution of single cell per cell area analyzed by Image J. Green circles, blue circles and red spheres represent control, 10SiNP (C and D), 100SiNP (E and F) and hydrogen peroxide treated cells respectively. Each symbol represents accumulated mitochondrial intensities of one single cell divided by its cell area for HuH-7 cells and SK-HEP-1 cells. (For interpretation of the references to color in this figure legend, the reader is referred to the web version of this article.)

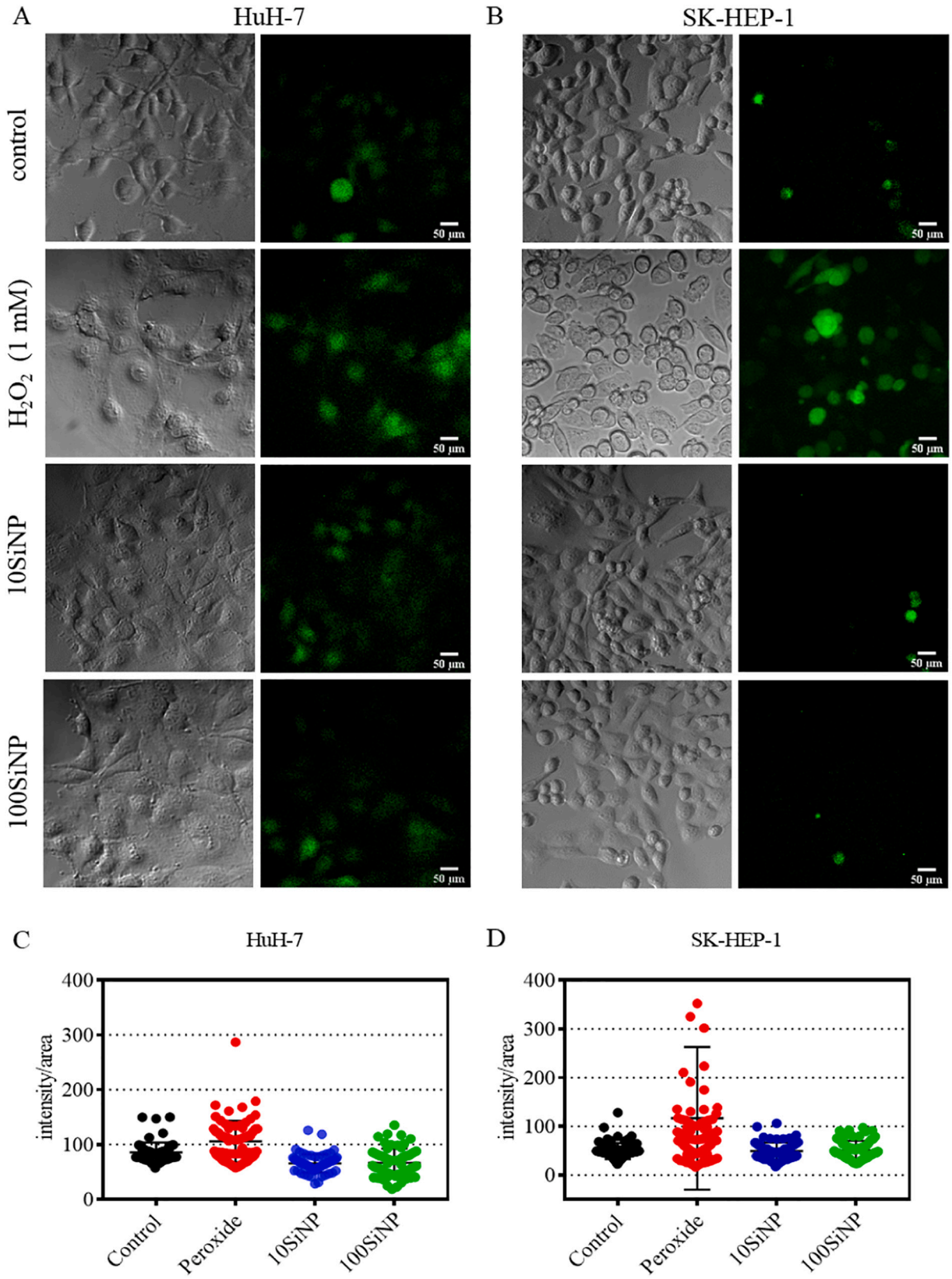

Fig. 5. Images of DCF-DA stained HuH-7 and SK-HEP-1 cell lines are shown (A and B) for ROS generation for control groups, peroxide treated, 10SiNP and 100SiNP treated cells. Non- fluorescent 10SiNP and 100SiNPs were used to eliminate spectral overlapping of FITC and DCF. Green colored cells indicated DCF fluorescence depending on the amount of ROS generated in the cells. The distribution of ROS intensity for individual cells was provided in C and D. (For interpretation of the references to color in this figure legend, the reader is referred to the web version of this article.)

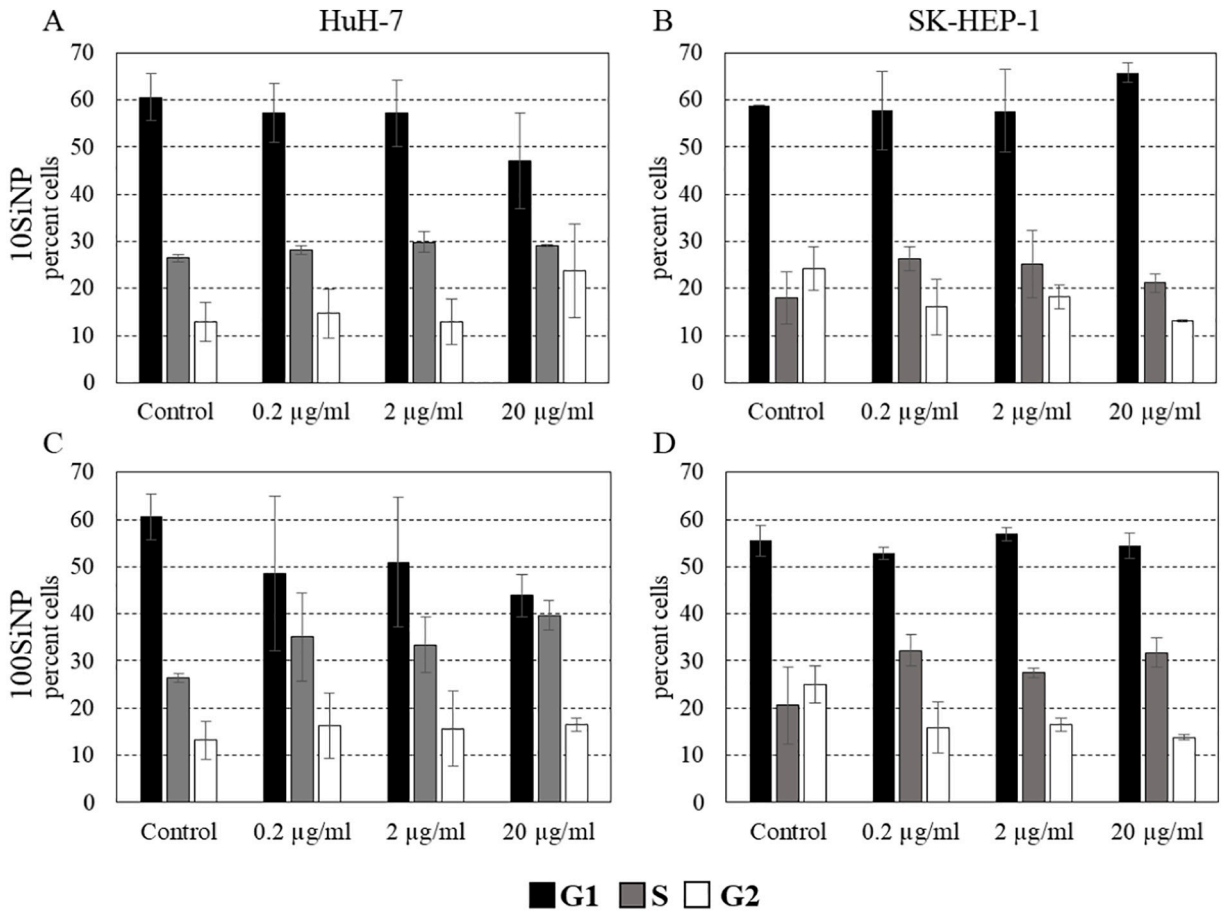

Fig. 6. The effects of 10SiNPs and 100SiNPs treatments on the cell cycle progression for HuH-7 (A and C) and SK-HEP-1 (B and D) cells were analyzed by flow cytometry. Peaks denoted the number of cells for the G0/G1 andG2/M phases. The graphs were illustrated for 72 h SiNP (up to 20 µg/ml) treatment for both cell lines. Dunnett's multiple comparisons test (Two-way ANOVA) was used for statistical analysis. There were no significant ($p > 0.05$) shifts between cell cycle phases based on Dunnett's multiple comparisons test(Two-way ANOVA) up to 72 h.

enter the cells because of their higher zeta potentials. Furthermore, the number of particles per given mass/volume for 10SiNPs is 10^3-fold higher than 100SiNPs due to size difference. The higher colocalization scores for 10SiNPs regardless of the cell type validate this hypothesis. We conclude that 10SiNPs create more interactions with cells and sub-organelles.

4.2. Biological responses of cells

We combined HuH-7 and SK-HEP-1 cells together as a hepatoblastoma and LSEC model to assess their biological responses to SiNPs. To the best of our knowledge, it is the first study using both cells together as a liver cancer model. HuH-7 cell line is a well-differentiated epithelial-like human hepatoblastoma cell line [23]. It has been used extensively as a physiologically relevant model to evaluate the effects of natural compounds, viruses and therapeutics on the liver [24–26]. SK-HEP-1 cells were derived from the ascitic fluid of a patient with liver adenocarcinoma [27]. These cells are considered as a cell model representing liver sinusoidal endothelial cells [28]. Liver sinusoidal endothelial cells form a barrier of the liver sinusoids and play a crucial role in substance exchange between hepatocytes and sinusoids.

When both cell lines were treated with SiNPs no adverse effects on the cell proliferation were measured either metabolic activity or cell density up to 5 days. They responded to SiNPs in the same way regardless of the particle sizes, the amount and the incubation time. Although a minimal decrease in the viability at 24 h was evaluated as statistically significant, no long-term effects was observed. Furthermore, the cell cycle analysis showed that SiNPs did not inhibit cell cycle progression. We did not observe any arrest in cell cycle phases for HuH-7 or SK-HEP-1 cells at 20 µg/ml at all incubation time.

It has been reported that SiNPs taken up by mammalian cells can induce direct physical or chemical damage or they can act indirectly (e.g., via inducing oxidative stress). There are contradictory data concerning whether or not SiNPs are genotoxic. Choi et al. 2011 demonstrated no mutagenicity of SiNPs (10 nm) in low concentration whereas in higher concentrations (100 and 150 µg/ml) the SiNPs were genotoxic [29]. Similarly, Demir et al. and Park MV et al. showed genotoxic effects of SiNPs as size, time and concentration-dependent manner [30,31]. Many of these studies used cancer cells or mouse cells for genotoxicity analysis. Because of the stability of their karyotype, low rate of spontaneous MN frequency, wild type p53 status and DNA repair capacity, it has been recommended to use primary human lymphocytes for MN detection as suggested in OECD guidelines (O.E.C.D. 2014).

To evaluate genotoxic effects of SiNPs we performed a micronucleus test in primary lymphocytes isolated from a healthy volunteer. Mitomycin C as appositive control generated an induction of approximately 50% MN. We analyzed at least 2000 nuclei to determine potential genomic damages. Since MNs can originate other nuclear anomalies we also analyzed NPBs and NBUDs formation. MN formation can originate from segregation errors in the anaphase induced by mis-repair or non-repair of DNA breaks, hypomethylation of repeat sequences in centromeric and pericentromeric DNA, defects in anaphase checkpoint genes whereas NPB and NBUD are biomarkers of genotoxic events and chromosomal instability [20]. Our results clearly showed that 10SiNP and 100SiNP did not induce any significant DNA damage in terms of MNi, NPB and NUBD frequencies independent of the

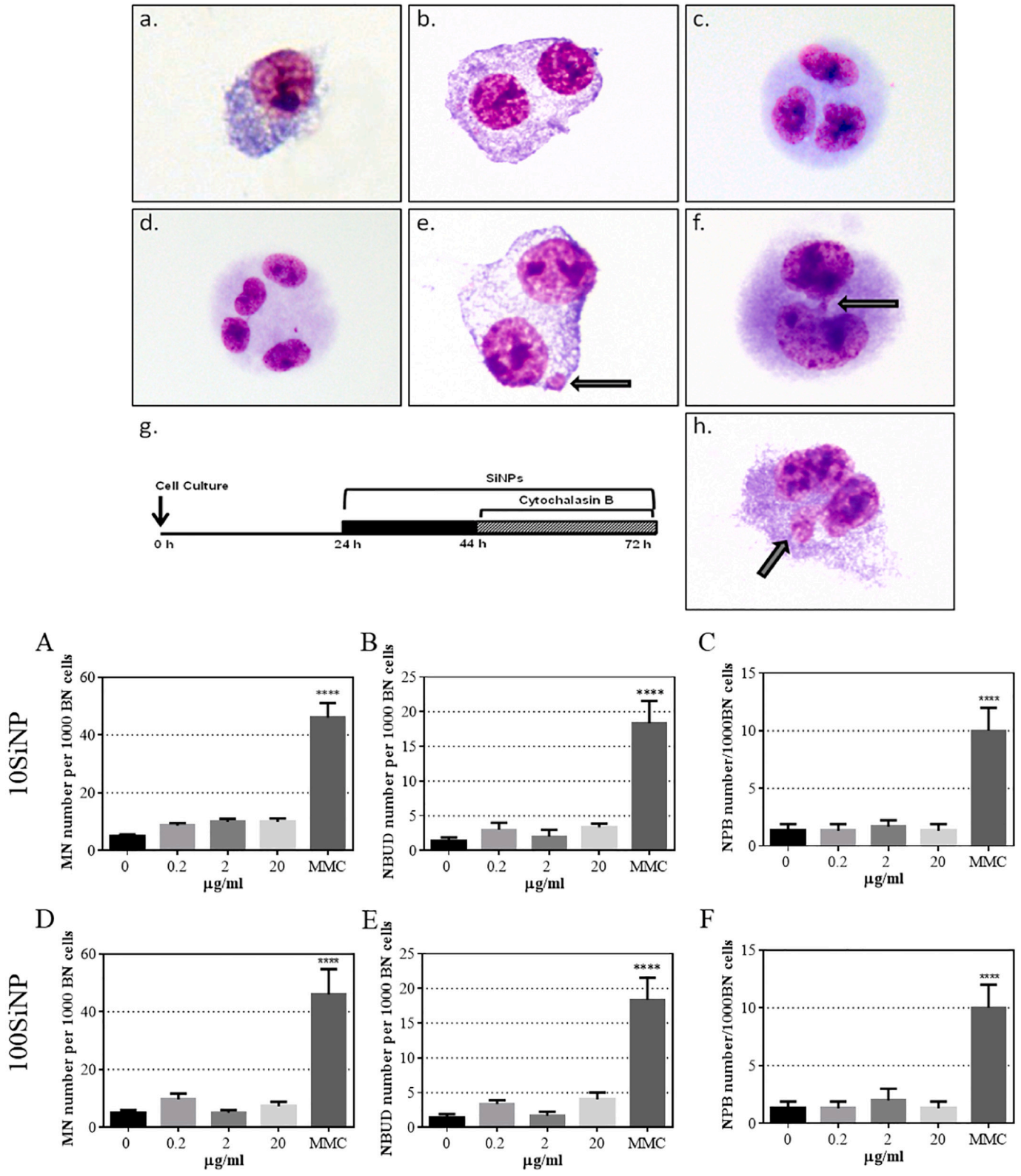

Fig. 7. Photomicrographs of the lymphocytes scored in micronucleus assay. Scored mononucleated (a), binucleated (b), trinucleated(c), multinucleated cells (d), micronuclei in binucleated cell (e), nucleoplasmic bridge (f), and nuclear bund (h) formations were illustrated.Cells were plated after isolation from whole human blood. SiNPs were added into the isolated cells and then incubated for 72 h. Cytochalasin B was added in order to block cytokinesis at 44 h as summarized in experimental diagram (g). The number of micronuclei, nuclear buds and nucleoplasmic bridges per 1000 binucleotide cells were recorded for after 10SiNPs and 100SiNPs treatment. Mitomycin (MMC*) was used as positive control. (****$p < 0.0001$).

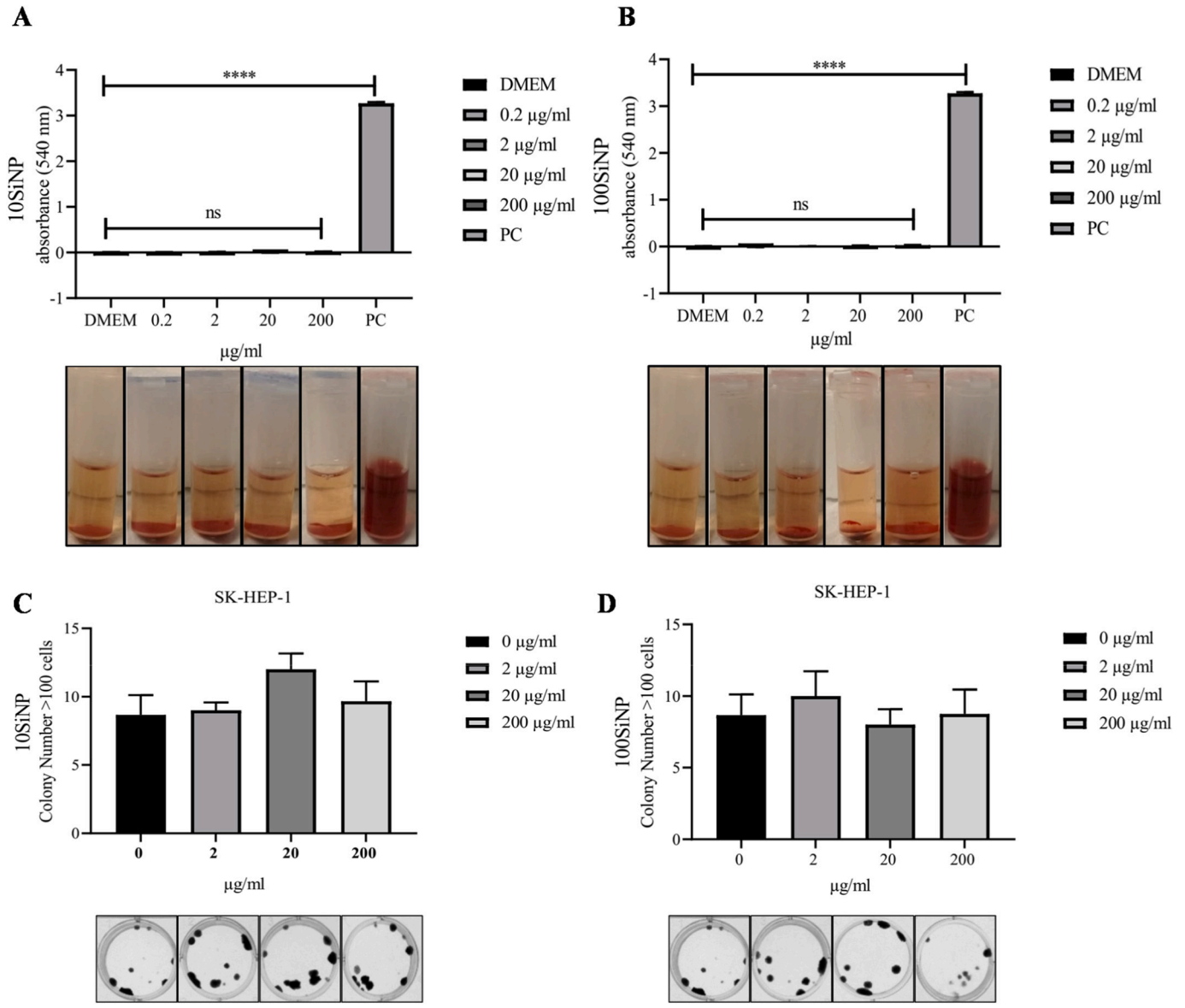

Fig. 8. Hemolytic activity of 10SiNP (A) and for 100SiNP (B) treatment. DMEM, 0.2 µg/ml, 2 µg/ml, 20 µg/ml, 200 µg/ml SiNP concentration and Triton X-100 was used as negative controls and positive control, respectively. OD values corresponding to each condition were presented at the top panel, tubes corresponding to each condition after centrifugation were shown at the bottom panel of Fig. 8A and B. There were not any statistical significant differences between DMEM, 0.2 µg/ml, 2 µg/ml, 20 µg/ml, 200 µg/ml 10SiNP and 100SiNP by one-way ANOVA ($p > 0.05$). There were statistical significant differences between Triton X-100 and 0.2 µg/ml, 2 µg/ml, 20 µg/ml, 200 µg/ml 10SiNP and 100SiNP by one-way ANOVA ($p < 0.05$). Colony numbers observed in clonogenic assay for SK-HEP-1 after treatment of DMEM, 0 µg/ml, 2 µg/ml, 20 µg/ml, 200 µg/ml 10SiNP (C) and 100SiNP (D (Top Panel)). Representative wells corresponding to these conditions were demonstrated below respectively (Bottom panel). Data are presented as mean ± standard deviation ($n = 4$).

incubation time and the amount of SiNPs used. Supporting MTT and SRB data no change in the NDI of the cells was detected in SiNPs treated cells compared to untreated ones.

As a positive control to confirm that mitochondria may respond to external induction, the liver cells were exposed to hydrogen peroxide in excess. The cells responded to hydrogen peroxide reducing cell size and diminishing MMP intensities. MMP, a result of charge gradient, is quantitatively expressed by the Nernst equation and proportional to the logarithmic fluorescent intensity ratio of mitochondria to the cytoplasm [32]. The mitochondrial respiration produces hydrogen peroxide and releases it to the cytoplasm. However, since the amount of hydrogen peroxide externally provided (1.0 mM) much higher than hydrogen peroxide amount (typically µM) released by mitochondria, the flow of hydrogen peroxide from mitochondria to cytoplasm is stopped, the charge gradient is reduced, as a result the MMP is lowered [33].

The surface of SiNPs covered by a corona layer neutralizes adverse effects of silanols on bare SiNP surfaces. The adverse effects as demonstrated in hydrogen peroxide treatment were not observed when SiNPs were used to treat the cells. We conclude that SiNPs do not interfere with mitochondrial processes and that SiNPs are safe for the mitochondrial respiration. MMP is typically −180 mV of a healthy mitochondrion [32] and assuming mitochondrion having an ellipsoid structure with dimensions of 100 × 500 nm, the effective mitochondrial membrane potential is estimated to be $-1.0\,\mu V/nm^2$. Taking the zeta potential of SiNPs in DMEM/FBS medium, it is more likely that 10SiNPs ($-2.72\,\mu V/nm^2$) will strongly interact with mitochondria compared to 100SiNPs ($-0.17\,\mu V/nm^2$). We propose that 10SiNPs are internalized and colocalized with mitochondria better than 100SiNPs (having lower colocalization scores compared to 10SiNPs).

Mitochondria response to cell division. Cell reduces its volume to

accumulate mitochondria closer to the nucleus for the energy-driven cell division processes. A closer inspection of Fig. 4 displays that a subgroup with higher MMP intensities and smaller cell area is gathered for the control and SiNP exposed cells, but not for the peroxide treated cells. This observation is in support of that SiNPs do not interfere with the cell division, and not leading to a cycle arrest.

At this point, the questions are where about SiNPs in the cytoplasm and should there be a lysosomal degradation? To answer, we inspected the colocalization scores of SiNPs with the lysosome. The colocalization coefficients of SiNPs with lysosomes were two-fold higher compared to the mitochondria for HuH-7 cells. This ratio was three-fold higher for the SK-HEP-1 cell line. The higher colocalization scores of SiNPs with lysosomes indicate that SiNPs are mostly accumulated in the lysosome and cannot escape from the endosomal internalization.

The increased amount of ROS alters homeostasis of the cell. The ROS generation was not increased by SiNP treatment however greater ROS production was observed following hydrogen peroxide treatment of the cells. Having almost the same ROS signal among the control group and SiNP treated cells suggest that SiNPs does not induce oxidative stress in the liver cancer cells.

Hemolysis of red blood cells was not varied upon exposure to SiNPs, showing that blood cells with oxygen are immune to nanoparticle perturbance. Blood is an enabling medium to convey drugs attached to nanoparticles to targeted cancer tissues, therefore biological stability of red blood cells carrying oxygen is vital for cancer treatment through ROS production.

5. Conclusions

We demonstrated that 10SiNP and 100SiNP regardless of size and amount did not induce cytotoxicity, cell cycle arrest, and inhibition of proliferation, mitochondrial damage, ROS generation and colony formation in the liver cancer cells. The SiNPs did not cause any difference in MN and NBUD frequencies in primary human lymphocytes, justifying the SiNPs are not genotoxic. Hemolytic activity of red blood cells was not changed due to SiNP treatment. We suggest that SiNPs may be a biosafe platform to carry drugs and genes to liver, and their ability to target cancer cells specifically may be improved further by decorating their solid surfaces with antibody fragments or peptides.

CRediT authorship contribution statement

Conceptualization: Serdar Özçelik.

Methodology: Serdar Özçelik, Neşe Atabey.

Data curation and Visualization: Özge Tüncel, Erkan Kahraman, Gülsün Bağcı.

Original draft preparation: Serdar Özçelik, Özge Tüncel.

Supervision: Serdar Özçelik, Neşe Atabey.

Writing- Reviewing and Editing: Serdar Özçelik, Neşe Atabey, Özge Tüncel.

Funding brought. Serdar Özçelik.

Declaration of competing interest

The authors declare that they have no known competing financial interests or personal relationships that could have appeared to influence the work reported in this paper.

Acknowledgements

This work was supported by the Izmir Institute of Technology [grant number 2012IYTEBAP06].

Appendix A. Supplementary data

Supplementary data to this article can be found online at https://doi.org/10.1016/j.msec.2020.111585.

References

[1] M.S. Bradbury, E. Phillips, P.H. Montero, S.M. Cheal, H. Stambuk, J.C. Durack, C.T. Sofocleous, R.J. Meester, U. Wiesner, S. Patel, Integr Biol (Camb) 5 (2013) 74–86.
[2] A.C. Anselmo, S. Mitragotri, Bioengineering & Translational Medicine 1 (2016) 10–29.
[3] Y.N. Zhang, W. Poon, A.J. Tavares, I.D. McGilvray, W.C.W. Chan, J. Control. Release 240 (2016) 332–348.
[4] L. Landgraf, D. Nordmeyer, P. Schmiel, Q. Gao, S. Ritz, S.G.J.S. Grass, S. Diabate, L. Treuel, C. Graf, E. Ruhl, K. Landfester, V. Mailander, C. Weiss, R. Zellner, I. Hilger, Sci Rep 7 (2017) 4341.
[5] G. Maiorano, S. Sabella, B. Sorce, V. Brunetti, M.A. Malvindi, R. Cingolani, P.P. Pompa, ACS Nano 4 (2010) 7481–7491.
[6] D. Napierska, L.C. Thomassen, D. Lison, J.A. Martens, P.H. Hoet, Part Fibre Toxicol 7 (2010) 39.
[7] Q. Mu, N.S. Hondow, L. Krzeminski, A.P. Brown, L.J. Jeuken, M.N. Routledge, Part Fibre Toxicol 9 (2012) 29.
[8] I.L.H. Annika Mareike Gramatke, Journal of Nanomedicine & Nanotechnology 05 (2014).
[9] C. Graf, Q. Gao, I. Schutz, C.N. Noufele, W. Ruan, U. Posselt, E. Korotianskiy, D. Nordmeyer, F. Rancan, S. Hadam, A. Vogt, J. Lademann, V. Haucke, E. Ruhl, Langmuir 28 (2012) 7598–7613.
[10] M. Benezra, O. Penate-Medina, P.B. Zanzonico, D. Schaer, H. Ow, A. Burns, E. DeStanchina, V. Longo, E. Herz, S. Iyer, J. Wolchok, S.M. Larson, U. Wiesner, M.S. Bradbury, J. Clin. Invest. 121 (2011) 2768–2780.
[11] M. Yu, J. Zheng, ACS Nano 9 (2015) 6655–6674.
[12] G. Durgun, K. Ocakoglu, S. Ozcelik, J. Phys. Chem. C 115 (2011) 16322–16332.
[13] H. Yuzugullu, K. Benhaj, N. Ozturk, S. Senturk, E. Celik, A. Toylu, N. Tasdemir, M. Yilmaz, E. Erdal, K.C. Akcali, N. Atabey, M. Ozturk, Mol. Cancer 8 (2009) 90.
[14] Terry L Riss, Richard A Moravec, Andrew L Niles, Sarah Duellman, Hélène A Benink, Tracy J Worzella, L. Minor, Eli Lilly & Company and the National Center for Advancing Translational Sciences, (2004).
[15] E. Owusu-Ansah, A. Yavari, U. Banerjee, (2008).
[16] A. Jeremy, P. Ingela, Cytometry Part A 77A (2010) 733–742.
[17] Piotr Pozarowski, Z. Darzynkiewicz, Methods Mol. Biol. 281 (2014) 301–311.
[18] M. Fenech, Nat. Protoc. 2 (2007) 1084.
[19] S.D. Niku, D.S. Hoon, A.J. Cochran, D.L. Morton, J. Immunol. Methods 105 (1987) 9–14.
[20] M. Fenech, M. Kirsch-Volders, A.T. Natarajan, J. Surralles, J.W. Crott, J. Parry, H. Norppa, D.A. Eastmond, J.D. Tucker, P. Thomas, Mutagenesis 26 (2011) 125–132.
[21] M.A. Dobrovolskaia, J.D. Clogston, B.W. Neun, J.B. Hall, A.K. Patri, S.E. McNeil, Nano Lett. 8 (2008) 2180–2187.
[22] X. Yang, Bio-protocol 2 (2012) e187.
[23] H. Nakabayashi, K. Taketa, K. Miyano, T. Yamane, J. Sato, Cancer Res. 42 (1982) 3858–3863.
[24] E.B. Lee, J.-H. Kim, W. Hur, J.E. Choi, S.M. Kim, D.J. Park, B.-Y. Kang, G.W. Lee, S.K. Yoon, Sci. Rep. 9 (2019) 1616.
[25] Z. Zhuo, J. Hu, X. Yang, M. Chen, X. Lei, L. Deng, N. Yao, Q. Peng, Z. Chen, W. Ye, D. Zhang, Sci. Rep. 5 (2015) 16185.
[26] M. Blanchet, C. Sureau, P. Labonte, Antivir. Res. 106 (2014) 111–115.
[27] S.C. Heffelfinger, H.H. Hawkins, J. Barrish, L. Taylor, G.J. Darlington, In vitro cellular & developmental biology: journal of the Tissue Culture Association 28a (1992) 136–142.
[28] X.Y. Li, Q.F. Luo, C.K. Wei, D.F. Li, L. Fang, Int. J. Clin. Exp. Pathol. 7 (2014) 92–100.
[29] H.-S. Choi, Y.-J. Kim, M. Song, M.-K. Song, J.-C. Ryu, Toxicol. Environ. Heal. Sci. 3 (2011) 7.
[30] E. Demir, V. Castranova, Toxicol. Rep. 3 (2016) 807–815.
[31] M.V.D.Z. Park, H.W. Verharen, E. Zwart, L.G. Hernandez, J. van Benthem, A. Elsaesser, C. Barnes, G. McKerr, C.V. Howard, A. Salvati, I. Lynch, K.A. Dawson, W.H. de Jong, Nanotoxicology 5 (2011) 168–181.
[32] S.W. Perry, J.P. Norman, J. Barbieri, E.B. Brown, H.A. Gelbard, BioTechniques 50 (2011) 98–115.
[33] S. Gáspár, Detection of Superoxide and Hydrogen Peroxide From Living Cells Using Electrochemical Sensors, Oxidative Stress: Diagnostics, Prevention, and Therapy, (2011), pp. 289–309.